INTERNATIONAL JOURNAL FOR NUMERICAL METHODS IN FLUIDS, VOL. 24, 477–492 (1997)

SOME EXPERIMENTS WITH STABILITY ANALYSIS OF DISCRETE INCOMPRESSIBLE FLOWS IN THE LID-DRIVEN CAVITY

J. J. GERVAIS, D. LEMELIN AND R. PIERRE

Département de Mathématiques et de Statistique, Université Laval, Québec, G1K 7P4, Canada

SUMMARY

We present results of a stability analysis of the lid-driven cavity flow based on classical C^0 finite element discretizations of the Navier–Stokes system. Using arc length continuation and subspace iteration to compute the eigenvalues of the tangent operator, we study the dependence of the bifurcation diagram and of the spectrum on the chosen discretization.

KEY WORDS: finite element; continuation; Hopf bifurcation

1. INTRODUCTION

In the recent past a lot of attention has been paid to the numerical analysis of the stability of certain incompressible flows using various techniques. However, even though a lot is known about the quality of velocity–pressure finite element discretizations of the incompressible Navier–Stokes equations for medium values of the Reynolds number, the question of their efficiency at predicting the correct behaviour of a flow in the neighbourhood of a bifurcation point has not often been considered. More precisely, in the course of a linear stability analysis of a given flow using the finite element method, how are the results, e.g. the bifurcation nature and value, affected by the choice of the discretization? This question will be the focal point of this paper, in which we intend to apply standard finite element techniques to the study of the linear stability of one of the incompressible flows which is most often used as a test problem, namely the lid-driven cavity flow.

Mathematically, the problem reads as follows: let $\Omega = (0, 1) \times (0, 1)$ be the flow domain; we look for a solution $(\mathbf{u}, p)$ of the stationary Navier–Stokes equations

$$\begin{aligned} -\frac{1}{\mathscr{R}}\Delta\mathbf{u} + (\mathbf{u}\cdot\nabla)\mathbf{u} + \nabla p &= 0, \\ \operatorname{div}\mathbf{u} &= 0, \\ \mathbf{u} &= (1,0) \quad \text{on } I = (0,1)\times\{1\}, \\ \mathbf{u} &= (0,0) \quad \text{on } \partial\Omega\backslash I. \end{aligned} \tag{1}$$

CCC 0271–2091/97/050477–16

Received 1 September 1993
Revised 31 May 1996

In the definition of the parameter $\mathscr{R}$, the Reynolds number, both the reference velocity and length are taken to be unity, so that $\mathscr{R}$ is nothing but the inverse of the kinematic viscosity.

Since we shall be more interested in the effect of the discretization than on the behaviour of the underlying dynamical system, we shall not use a time-dependent model and shall confine ourselves to the analysis of bifurcations from the stationary state. Among these, there could be bifurcations to an unsteady state to which the time-independent system is insensitive. In order not to miss them, we shall study the variation of the spectrum of the tangent operator along the paths of solutions. Typically, in such a problem where no symmetry is obviously present, we expect to observe either standard limit points or bifurcation to a periodic solution, i.e. Hopf bifurcation. The possible appearance of a Hopf bufurcation for the lid-driven cavity flow has been an open question for a while.[1] That such a bifurcation can indeed be detected by numerical methods is not altogether clear. However, if the continuous problem undergoes a Hopf bifurcation, it will typically be persistent; hence all sufficiently small perturbations of the flow should exhibit the same behaviour. The usual way of detecting this phenomenon is to compute a sequence of critical values of the Reynolds number that converges to the real one as the mesh size goes to zero. Some results, obtained with spectral methods applied to regularized boundary conditions,[2] gave strong indications that in the case under consideration the continuous system was indeed bifurcating to a periodic flow. This conclusion is supported by a recent work[3] which presents a thorough comparison between the results obtained through spectral analysis and those obtained by direct simulation using a time-dependent finite element code. The results that we are going to present here will confirm the correctness of the numerical values presented in that paper.

However, our real contribution to these questions will not be the determination of the critical values. Rather, we shall concentrate on the analysis of the influence of the two most important numerical parameters associated with a finite element discretization, namely the mesh and the element. Using the popular Mini and Taylor–Hood discretizations, we shall give examples of spurious limit points and spurious Hopf bifurcations. The commonly recommended cure to this problem is mesh refinement, but we shall show that it might very well be impossible to implement it because of hardware requirements. In this respect it will turn out that the continuous pressure discretization is more demanding than the discontinuous one, this being particularly the case with first-order elements. Not surprisingly, we shall be able to relate this difference to the incompressibility condition. Thus, while we do not introduce any innovative technique, we nevertheless hope that our remarks, which might very well be valid for other types of discretization, will prove useful and will prompt research on the development of good theoretical tools to compare the finite element discretizations of incompressible flows at very high Reynolds numbers.

The rest of the paper is organized in the following way. In Section 2 we briefly review the basic numerical schemes: Newton's method, pseudo-arc length continuation and subspace iteration. In Section 3 we recall some facts from stability theory, in Section 4 we present our most typical results and we conclude in Section 5.

2. BASIC NUMERICAL SCHEMES

Our notation is standard. Problem (1) is set in the spaces

$$V = (H_0^1(\Omega))^2, \qquad Q = L_0^2(\Omega). \tag{2}$$

To discretize (1), we first partition Ω with a finite element grid $\mathscr{T}_h$ which will always consist of triangles. On this grid we may define the finite element P_1 and P_2 spaces

$$X_h^k = \{w_h \in C^0(\Omega) | w_h|_K \in P_k(K), \forall K \in \mathscr{T}_h\}, \quad k = 1, 2,$$

and the bubble space

$$\mathscr{B}_h = \left\{ \sum_{K \in \mathscr{T}_h} \mathbf{v}_K \phi_K | \mathbf{v}_K \in \mathbb{R}^N, \forall K \right\}. \tag{3}$$

Here ϕ_K is either the standard cubic bubble

$$\phi_K = 27\lambda_1\lambda_2\lambda_3 \tag{4}$$

or the non-conforming quadratic bubble

$$\phi_{K,\mathrm{nc}} = 2 - 3(\lambda_1^2 + \lambda_2^2 + \lambda_3^2), \tag{5}$$

where the λ_i are the barycentric co-ordinates. With these spaces we can build two conforming approximations of $V \times Q$, namely $V_h \times Q_h$, where

$$V_h = \begin{cases} ((X_h^1)^2 \cap V) \oplus \mathscr{B}_h & \text{for } k = 1, \\ (X_h^2)^2 \cap V & \text{for } k = 2, \end{cases} \tag{6}$$

$$Q_h = X_h^1, \quad k = 1, 2. \tag{7}$$

The case $k = 1$ is a possible Mini discretization,[4,5] whereas the case $k = 2$ is the popular Taylor–Hood discretization,[6] hereafter denoted P2P1. It has been known for a while[5,7] that the addition of local stabilizing functions to the P1P1 discretization (or, for that matter, to any $P_k - P_k$ discretization) is equivalent to using a streamline upwind Petrov–Galerkin (SUPG) method in which the value of the upwind parameter depends explicitly on the choice of the bubble.

We shall also consider the simple modification of P2P1 which corresponds to

$$Q_h = X_h^1 \oplus \{q_h | q_h|_K \in P_0(K), \forall K \in \mathscr{T}_h\}.$$

The interest of this modification is that it imposes local mass conservation on the velocity fields, i.e.

$$\int_K \mathrm{div}\,(\mathbf{v}_h)\mathrm{d}\mathbf{x} = 0, \quad \forall \mathbf{v}_h \in V_h, \quad \forall K \in \mathscr{T}_h.$$

The importance of this condition for some other incompressible flow problems was recognized a long time ago and the above modification of the Taylor–Hood element has been advocated in References 8 and 9. Different stability analyses of the corresponding mixed formulation of the Stokes problem have been proposed in References 10 and 11. In the following this discretization will be termed P2P1P0.

Since we use conforming approximations of the primitive variable spaces, we can consider the standard variational approximations of (1) given by

$$\begin{aligned} &\frac{1}{\mathscr{R}} \int_\Omega \nabla \mathbf{u}_h : \nabla \mathbf{v}_h \mathrm{d}\mathbf{x} + \int_\Omega (\mathbf{u}_h \cdot \nabla)\mathbf{u}_h \cdot \mathbf{v}_h \mathrm{d}\mathbf{x} - \int_\Omega p_h \mathrm{div}\, \mathbf{v}_h \, \mathrm{d}\mathbf{x} = 0, \quad \forall \mathbf{v}_h \in V_h, \\ &\int_\Omega \mathrm{div}\, \mathbf{u}_h q_h \mathrm{d}\mathbf{x} = 0, \quad \forall q_h \in Q_h, \\ &\mathbf{u}_h = \mathbf{g} \quad \text{on } \Gamma. \end{aligned} \tag{8}$$

The boundary function **g** being piecewise linear, boundary conditions can be treated in the usual way. The reader will notice the fact that we are considering the 'contained flow' case, i.e. $u(0, 1) = u(1, 1) = 0$. The reason for this is that, in so doing, we can use arbitrary meshes without having problems in verifying the discrete flux condition

$$\int_\Gamma \mathbf{g} \cdot \mathbf{n} \, d\mathbf{x} = 0$$

that should be satisfied for problem (8) to be well posed.

Problem (8) is a non-linear problem that could be solved with many different techniques. In view of the fact that we intend to use continuation and do some monitoring of the eigenvalues of the tangent matrix, we will resort to the standard Newton method which is known to behave well with our choice of spatial discretizations.[12] Thus a typical step of our iterative method will consist of solving the following linear system: given $(\mathbf{u}_n, p_n)$, find $(\mathbf{u}_{n+1}, p_{n+1})$ such that

$$\begin{aligned}
&\frac{1}{\mathscr{R}} \int_\Omega \nabla \mathbf{u}_{n+1} : \nabla \mathbf{v}_h \, d\mathbf{x} + \int_\Omega (\mathbf{u}_{n+1} \cdot \nabla) \mathbf{u}_n \cdot \mathbf{v}_h \, d\mathbf{x} + \int_\Omega (\mathbf{u}_n \cdot \nabla) \mathbf{u}_{n+1} \cdot \mathbf{v}_h \, d\mathbf{x} - \int_\Omega p_{n+1} \operatorname{div} \mathbf{v}_h \\
&\qquad = \int_\Omega (\mathbf{u}_n \cdot \nabla) \mathbf{u}_n \cdot \mathbf{v}_h \, d\mathbf{x}, \quad \forall \mathbf{v}_h \in V_h, \\
&\int_\Omega \operatorname{div} \mathbf{u}_{n+1} q_h \, d\mathbf{x} = 0, \quad \forall q_h \in Q_h, \\
&\mathbf{u}_{n+1} = \mathbf{g} \quad \text{on } \Gamma.
\end{aligned}$$

In matrix form this system will become

$$\begin{pmatrix} \mathbf{A} + \mathbf{L}(\mathbf{u}_n) & -\mathbf{B}^T \\ \mathbf{B} & \varepsilon \mathbf{M} \end{pmatrix} \begin{pmatrix} \mathbf{u}_{n+1} \\ p_{n+1} \end{pmatrix} = \begin{pmatrix} \mathbf{F}(\mathbf{u}_n) \\ \mathbf{G} \end{pmatrix}, \tag{9}$$

where **A** is the vector viscosity matrix, **B** is the discrete divergence, $-\mathbf{B}^{\mathrm{T}}$ is the discrete gradient and $\mathbf{L}(\mathbf{u}_{\mathrm{n}})$ is the sum of the convection terms. On the right-hand side the vector **G** depends only on the boundary conditions. The matrix **M** is the pressure mass matrix and its addition to the system corresponds to the use of a penalty approach when $\varepsilon \neq 0$. The reason we sometimes introduce this perturbation has to do with our matrix storage and node numbering, which result in zero pivot in the case where the storage forbids pivoting. This way of getting around that problem is amply described and motivated in Reference 12, Section 4. When the P2P1P0 discretization is used, the constant part of the pressure will be condensed at the element level and never recovered. The effect of this modification will be the addition to the Laplacian matrix of a matrix **D**, the elements of which are of the form

$$D_{i,j} = \frac{1}{\varepsilon} \sum_{K \in \mathscr{T}_h} \int_K \operatorname{div} (\mathbf{v}_i) \, d\mathbf{x} \int_K \operatorname{div} (\mathbf{v}_j) \, d\mathbf{x},$$

where the $\mathbf{v}_i$ are the basis functions. This modification is readily made at the elementary matrix computation level and requires no other transformation of the P2P1 code whatsoever.

Remark 1

(a) In the case of the Mini element the use of a penalty term is not compulsory because of the fact that static condensation of the local degrees of freedom modifies the tangent matrix in such a way as to eliminate zeros along the diagonal. This property allowed us to test the effect of the penalization on the structure of the spectrum. We found it to be negligible.

(b) The main reason we did not consider the use of a quasi-Newton algorithm is that, from our experience, the cost of finding the Navier–Stokes solution is small compared with that of determining the eigenvalues of the tangent matrix. This is partly due to the fact that, since we use continuation, we are, most of the time, near enough the solution at the start to be able to capture it in much less than 10 Newton iterations.

(c) There would be different possibilities to solve system (9). However, at high Reynolds number and in the vicinity of a bifurcation point the tangent matrix will be almost singular, which means that the use of an iterative procedure could become prohibitive. In particular, we tested some preconditioned GMRES algorithms and found that, in this range of the parameter, no elementary preconditioner (diagonal or block diagonal) could do the job. This question of the construction of an effective preconditioner will require more attention. As a consequence of the above difficulty, we resorted to direct LU decomposition and found it to be very robust.

To complete the description of our implementation of the Newton algorithm, we discuss the question of the starting procedure. For this we have used both incremental and continuation methods. The first one is completely standard. As to the second, which is now widely used in conjunction with Newton or quasi-Newton methods when applied to non-linear problems, its application to the analysis of the lid-driven cavity flow goes back at least to Reference 13, where it was combined with a finite difference spatial discretization. It has also been used in Reference 14, for the same test problem, in conjunction with a C^0 finite element discretization of the streamfunction–vorticity mixed variational formulation. In this last paper the pseudo-arc length continuation procedure was coupled with a least squares solver, but the goal was not the analysis of the flow at high Reynolds number, rather the numerical analysis of the least squares method itself. The application appears to have been limited to coarse meshes and low Reynolds numbers, i.e. $\mathscr{R} \in [0, 2000]$.

The approach that we have favoured is based on the introduction of a pseudo-arc length parameter s determined by a pseudo-arc length equation. The solution of the resulting augmented system is obtained with an algorithm which couples a Euler-type predictor for the computation of the initial value to our Newton corrector. The linear systems to be solved at each Newton iteration are then bordered versions of (9) which are solved by block elimination. A complete description of the method can be found in Reference 15. We shall content ourselves with one more specific comment. The main reason we are interested in this approach is that the use of a Euler-type predictor based on an approximate computation of the tangent vector enables us to select a starting value of $(u, p, \mathscr{R})$ at each Δs-step, even in the neighbourhood of a critical point. These predicted values being, for small Δs, well within the domain of attraction (in the sense of Newton's method) of the solution of the Navier–Stokes system that exists on the branch of solutions under consideration, the method converged fast and we were able to follow that branch and to step over limit points.

The last algorithm on which we must give information is the one used for the eigenvalue computation. In this type of problem the size of the matrix together with the fact that it is non-symmetric is usually considered as the main difficulty. In our context this difficulty is amplified by the fact that the matrix itself is not known explicitly. To make this point clearer, we go back to the formulation (9) of the linear problems. It is not the spectrum of the full matrix that we are interested in, neither is it that of the matrix $\mathbf{A} + \mathbf{L}(\mathbf{u}_n)$. Rather, we want to compute the eigenvalues and eigenvectors of the restriction of the operator $\mathrm{A} + \mathbf{L}(\mathbf{u}_n)$ to the subspace of V_h consisting of vectors whose discrete divergence is zero. Namely, we want to restrict that operator to the space

$$\ker\mathbf{B} = \left\{ \mathbf{v}_h \in V_h \middle| \int_\Omega \operatorname{div} \mathbf{v}_h q_h \, \mathrm{d}\mathbf{x} = 0, \forall q_h \in Q_h \right\}.$$

Although, for the Taylor–Hood case, explicit local bases of ker **B** can effectively be built,[16] their use is somewhat complicated and would require a new assembly. Moreover, to our knowledge, no such basis is known for the Mini element. This being the case, we choose a method which does not require the explicit construction of the matrix, namely the well-known subspace iteration method.[17] A detailed description of the application of this algorithm to the detection of bifurcation of incompressible fluids is given in Reference 18, so we shall limit ourselves to a few more specific comments.

We have applied this algorithm to the computation of the k smallest eigenvalues in the spectrum, i.e. the k biggest of the inverse operator. This means that each matrix–vector product required by the algorithm amounts to solving the constrained variational problem

$$a_{\mathscr{R}}(\mathbf{v}_h, \mathbf{w}_h) = (\mathbf{u}_n, \mathbf{w}_h), \quad \forall \mathbf{w}_h \in \ker \mathbf{B},$$

where the bilinear form $a_{\mathscr{R}}$ is the one associated to $\mathbf{A} + \mathbf{L}(\mathbf{u}_n)$, with $\mathbf{u}_n$ the velocity solution. Introducing a Lagrange multiplier, we can replace this problem by

$$\begin{aligned} a_{\mathscr{R}}(\mathbf{v}_h, \mathbf{w}_h) - (p, \operatorname{div} \mathbf{w}_h) &= (\mathbf{u}_n, \mathbf{w}_h), \quad \forall \mathbf{w}_h \in H_h, \\ (\operatorname{div} \mathbf{v}_h, q) &= 0, \quad \forall q \in Q_h. \end{aligned}$$

In matrix form this system is nothing but (9) with $(\mathbf{F}, \mathbf{G}) = (\mathbf{M}_v \mathbf{U}, 0)$, where $\mathbf{M}_v$ is the vector velocity mass matrix and $\mathbf{U}$ is the vector of degrees of freedom of $\mathbf{u}_h$. To solve these systems, we use the last LU decomposition produced by the Navier–Stokes solver; hence there is no new assembly required at this step. As to the matrix $\mathbf{M}_v$, it is assembled once and for all at the beginning, also with skyline storage.

The implementation of the algorithm that we have used is the EB12 code of Duff and Scott.[19] We were mainly interested in two of the features of this code. The first one is its capacity of deflation, i.e. locking the converged eigenvectors, typically those corresponding to the dominant eigenvalues, while it pursues iteration for the other ones: this time-saving quality was our first motivation to abandon our home-made version of the algorithm.

The second interesting feature of the EB12 code is its capacity to replace the polynomials $p(z) = z^n$ in the underlying power method by other 'filters' in order to select groups of eigenvalues other than the biggest ones in modulus. Indeed, those we are really interested in are the leftmost ones. Hence, if we look for the k smallest, we have to choose k big enough to be sure that those of smallest real part fall in the computed group. In the absence of information on those eigenvalues there is no way to compute an appropriate k; thus one is forced to overestimate it. This leads to quite a bit of extra work. A lot of research has been done on this question and we have tested a few of the ideas proposed in the literature to get around the problem, in particular the very nice ideas advocated by Cliffe, Garratt and Spence which are based on the use of conformal transformations. All of them failed! A summary of our conclusions is given in Reference 3, so here we shall be brief. The solution to this problem advocated in EB12 is to use Chebychev filters on appropriate ellipses which are constructed in such a way as to contain the unwanted eigenvalues.[20] Although we do not have a definite explanation as to why this failed in our case, we believe that it could be partly attributed to the spectrum geometry. In the lid-driven cavity case there are very many eigenvalues in a narrow band to the right of the imaginary axis. For an ellipse to contain some of these eigenvalues but not all of them, it would have to be very elongated. This could be one of the eigenvalue distributions for which Saad himself reports difficulties in the ellipse parameter determination. In any case we could not use this capacity of the code, but we were very satisfied with its careful monitoring of the residuals and its restarting capability.

3. STABILITY ANALYSIS AND CONTINUATION

The analysis presented below is based on the so-called principle of linearized stability,[21,22] which can be summarized as follows. Let $\Sigma(\mathscr{R})$ denote the spectrum of the tangent operator of the Navier–Stokes system computed at a given solution $(\hat{\mathbf{u}}, \hat{p})$ corrresponding to a given Reynolds number $\mathscr{R}$. This solution is asymptotically stable if

$$\xi(\mathscr{R}) := \inf_{\sigma \in \Sigma} \mathrm{Re}(\sigma) > 0$$

and unstable if $\xi(\mathscr{R}) < 0$.

It is known that for small enough $\mathscr{R}$ there exists a unique stationary solution, called the basic flow, and that it is asymptotically stable. In fact, the basic flow is globally asymptotically stable (all perturbations decay to zero as $t \to \infty$) if $\mathscr{R}$ is small enough.[21] As $\mathscr{R}$ increases, the basic flow may lose that property but still remain asymptotically stable, until $\mathscr{R}$ reaches a critical value at which it loses stability altogether. This value $\mathscr{R}_c$ is precisely the one for which $\xi(\mathscr{R})$ changes sign.

For flows in a bounded domain we have the following results for the spectrum $\Sigma(\mathscr{R})$.[22]

(1) $\Sigma(\mathscr{R})$ contains only isolated eigenvalues with finite multiplicities.
(2) The eigenvalues depend continuously on $\mathscr{R}$.
(3) The eigenvalues are in the interior of a parabola of the form

$$x = \frac{1}{4c} y^2 - c, \quad \text{where } c > 0.$$

We thus deduce that at a critical Reynolds number we have a finite number of eigenvalues on the imaginary axis. Therefore, in general, loss of stability will occur in one of the following situations.

(i) One real eigenvalue changes sign as $\mathscr{R}$ varies across $\mathscr{R}_c$.
(ii) A pair of complex conjugate eigenvalues crosses the imaginary axis as $\mathscr{R}$ varies across $\mathscr{R}_c$.

In our physical situation there is no geometric symmetry in the flow and the eigenvalues will typically be simple. Moreover, even though other theoretical situations may occur (in the presence of a $\mathbb{Z}^2$ symmetry for example), the expected dynamical behaviour corresponding to the above two cases would be the following. In case (i) the solution is a limit point, i.e. a turning point of the branch of solutions which lose their stability as that point is crossed. In case (ii) we have a Hopf bifurcation with a transition to a periodic solution which will be stable if the bifurcation is supercritical and unstable if it is subcritical.

Some remarks ought to be made about the behaviour of the numerical method in these two different situations. In the first case the tangent matrix becomes singular and the tube of convergence of Newton's method shrinks into a cone. This is where continuation plays a role and helps us both to get near the critical point and to step over it. However, if we take big steps, the bifurcation may very well go unnoticed and we could wrongly conclude that the stationary solution is still dynamically stable. In the second case, nothing happens; the tube of convergence is unaffected. Monitoring the spectrum of the tangent matrix is then compulsory if we want to capture the bifurcation and predict the correct frequency of the periodic solution (without time integration). A good approximation of that frequency just after the bifurcation point is given by

$$f \approx \frac{|\mathrm{Im}(\sigma)|}{2\pi}, \tag{10}$$

where σ is one of the critical eigenvalues.[23] This is the best information that we can deduce from our spectral computation, since from our 'stationary' point of view there is no way to determine whether

the bifurcation is sub- or supercritical. Finally, we remark that, since the spectrum is limited by a parabola, we can hope that the critical eigenvalues will not be too far from the origin. How near is 'not too far' is quite another question. In our context, numbering the eigenvalues from the smallest one in modulus, the critical ones were in the first 250. Of course, our computational approach does not insure that these eigenvalues are the first to cross the axis, but the time-dependent simulation presented in Reference 3 confirms it.

4. NUMERICAL RESULTS

In this section we shall present results obtained with discretizations of the type (6), (7) and various meshes.

4.1. Effect of discretization on values of $\mathscr{R}_c$

As a first step we comment on some preliminary results obtained with different discretizations. Using the Newton algorithm as such, without any continuation, we start from the solution at $\mathscr{R} = 1$, incrementing the parameter up to the first 'critical' value, which we first naively define as the value for which we lose convergence of Newton's method. According to the discussion in Section 2, this value would normally correspond to a limit point and there is nothing that insures that we have not passed by a Hopf bifurcation. We might also pass a limit point by taking sufficiently large Reynolds number steps or we might lose convergence only because the solution varies a lot on a small Reynolds number interval, which makes the selection of the initial value for Newton's method very hard.

In Figures 1, 2 and 3 (left) we have represented five meshes on which these tests were conducted. The first one is a structured mesh of 2500 elements obtained by partitioning the flow domain into N^2 equal squares, each of which is then split into four equal triangles. The next three are unstructured meshes with refinements in the corners. The last one is also regular but with a concentration of triangles along the boundaries in order to get more information both from the boundary layer and from the corner vortices. Such meshes are easily obtainable in the following way: we partition the flow domain into N^2 equal squares; each of these squares is then split into two or four equal triangles, which leads to a regular mesh that looks like the first one; the boundary-refined mesh is finally defined as the conformal image of the regular mesh by the mapping

$$X(i) = \sin^2\left(\frac{\pi}{2}x(i)\right), \qquad Y(i) = \sin^2\left(\frac{\pi}{2}y(i)\right).$$

In the sequel these meshes will be denoted by cav2sin[n] for the case of two triangles per square and cavsin[n] for the case of four.

Let us first consider results obtained with the Mini discretization. On the structured mesh of 2500 elements, which looks very much like a finite difference mesh, we were able to push the computation up to $\mathscr{R} = 81{,}360$. As seen in Figure 3 (right), at such a high Reynolds number the numerical solution is highly non-physical. On the first unstructured mesh, which is rather symmetric and comprises 2886 elements, we lost convergence at $\mathscr{R} = 4960$, which is very far from the 'critical' Reynolds number of the preceding example even though the number of elements is comparable. For the other two unstructured meshes, respectively of 3338 and 3754 elements and which are refined at the location of the first Moffat eddy,[24] we again got two rather different 'critical' Reynolds numbers, namely $\mathscr{R}_c = 9325$ in the first case and $\mathscr{R}_c = 11{,}145$ in the second. It should be observed that from both a qualitative and a quantitative point of view these two meshes are rather similar but nevertheless

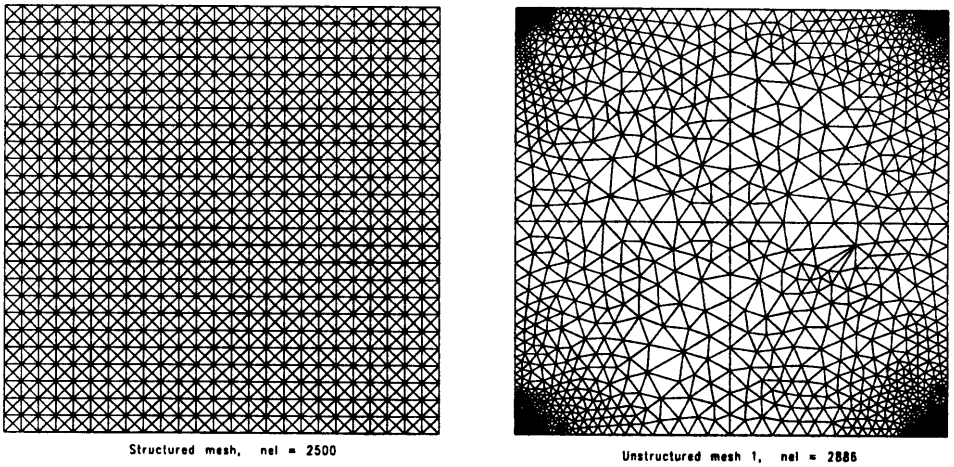

Figure 1. Meshes

predicts a very different qualitative behaviour of the solutions, at least from the point of view of the convergence of Newton's method.

In order to analyse the effect of the element selection, we repeated the above test on the cavsin[21] mesh using the Taylor–Hood discretization and the Mini discretization with both bubbles (4) and (5). On this mesh, the conforming Mini discretization gives a 'critical' Reynolds number $\mathscr{R}_c = 20{,}406$, the non-conforming one $\mathscr{R}_c = 9860$ and the Taylor–Hood discretization $\mathscr{R}_c = 8760$. We shall see that in this last case the 'critical' Reynolds number is way beyond the first limit point, which suggests, as is indeed the case, that the branches of multiple discrete solutions are very near to one another. It is also interesting to note that the use of the quadratic bubble leads in this case to results which are much nearer to those given by the P2 discretization than does the use of the cubic bubble.

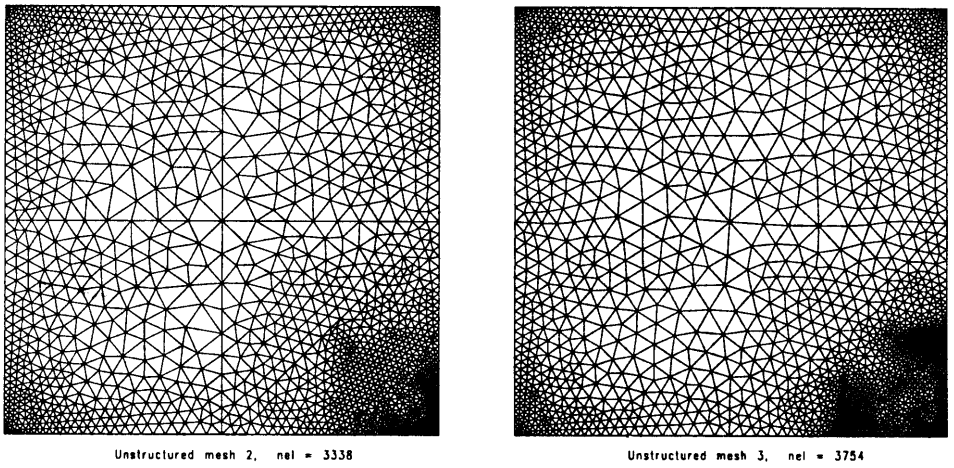

Figure 2. Meshes

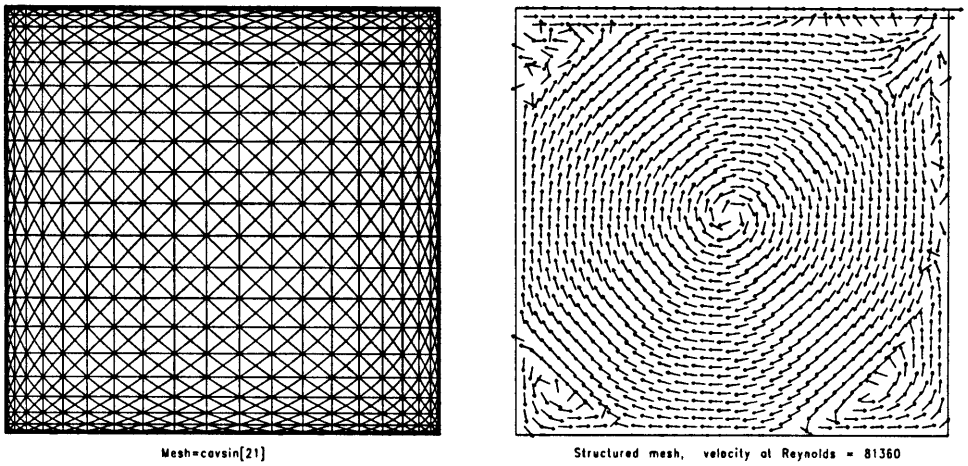

Figure 3. Cavsin mesh (left). Solution with Mini (right)

Remark 2

For further reference it will be useful to state the relationship between the number of elements and the number of velocity degrees of freedom for the discretizations for which we are going to present results. In Table I, n is the number of squares; hence the number of elements is $2n^2$ for cav2sin and $4n^2$ for cavsin.

It is interesting to note that, since in the Navier–Stokes context one is using the bubble velocity degrees of freedom of the Mini element, this gives a richer approximation of the velocity field than the P1P1 approximation that corresponds to the standard SUPG regularization of Hughes and Franca,[25] even though the linear part of the Mini approximation coincides with the SUPG solution.[7] Indeed, Table I confirms that the number of velocity degrees of freedom of Mini is much nearer to that of P2P1 than to that of P1P1.

4.2. Some bifurcation diagrams

A study of bifurcation diagrams of the steady state Navier–Stokes equations in the lid-driven cavity has been presented in Reference 26, where the computations were done with a finite difference scheme applied to the streamfunction–vorticity formulation of the system. Using that method, Schreiber and Keller have exhibited diagrams containing mesh-dependent limit points that are merely numerical. To ascertain their numerical nature, they have computed solutions on increasingly finer meshes, obtaining diagrams which appear to be qualitatively identical but on which the limit points were pushed towards ∞ as the mesh parameter went to zero. In Reference 27 a similar study was conducted for a flow in a widening channel and a great variety of numerical limit points was also observed. Nevertheless, in this last work the refinement process was not only pushing these points to the right but was also creating new limit points in such a way that the diagrams were not topologically

Table I. Numbers of degrees of freedom

	P1P1	Mini	P2P1
Cav2sin	$2n^2 - 4n + 2$	$6n^2 - 4n + 2$	$8n^2 - 8n + 2$
Cavsin	$4n^2 - 4n + 2$	$12n^2 - 4n + 2$	$16n^2 - 8n + 2$

equivalent. We have encountered a similar situation with our discretization of the lid-driven cavity. We follow References 1, 26 and 27 and use the H^1 seminorm ($|\mathbf{u}_h|_1^2$) versus $\mathscr{R}$ to represent the diagrams. In Figure 4 and 5 (left) we have represented the bifurcation diagrams obtained with the Taylor–Hood element and the cav2sin[21], cav2sin[29] and cavsin[21] meshes. The corresponding numbers of degrees of freedom are to be found in Table I. In each of those diagrams the curve starts from the endpoint identified by an S and the markers indicate the points corresponding to one value of the arc length parameter. Note that the crossing points of the branch are not bifurcation points but are caused by the projection of the branch on a two-dimensional space.

As to the parameter step, it was variable and adjusted manually. This means that we would use a large $\Delta s(\approx 100)$ whenever possible but would reduce its value as soon as the initial approximation predicted by the Euler step fell out of the attraction basin for the next solution. Around a limit point we often had to use quite a small Δs of about 10^{-1}. The diagram corresponding to the cav2sin[21] mesh exhibits four limit points for values of the Reynolds number ranging from 3100 to 4700. The first limit point exhibited is the first encountered, but the last one shown could very well not be the last one on the curve. Similar remarks apply to the second diagram, which is nevertheless very different from the first, showing seven limit points in a range of [5800, 8400] for the Reynolds number. As was the case in Reference 26, the first limit point has been pushed to the right by an amount $\Delta\mathscr{R} \approx 2200$, but the two diagrams are very different. This tendency is confirmed by the third diagram, on which the first limit point appears at $\mathscr{R} \approx 8230$ and which shows five limit points in the short range [8000, 8400]. In this last case also we cannot guarantee that we have computed all the limit points. As a matter of fact, it seems that the next part of the curve is turning very sharply, because we could not pass the last value even with small Δs. It is important to recall that the incremental method allowed us to pass that region rather easily by taking a large Reynolds step at $\mathscr{R} = 8200$, confirming the fact that loss of convergence of an iterative method, be it Newton or any other, says little about the nature of the bifurcation diagram.

4.3. Eigenvalue behaviour

In this last subsection we want to analyse the influence of the discretization on the behaviour of the spectrum of the tangent matrix. To this end we shall use the spectrum computed in Reference 3 as a reference. This choice is justified by the fact that its quality has been assessed both by careful mesh refinements and by direct time-dependent simulation. The topology of this spectrum is very peculiar and quite intriguing: in a rather large band to the right of the imaginary axis the eigenvalues are

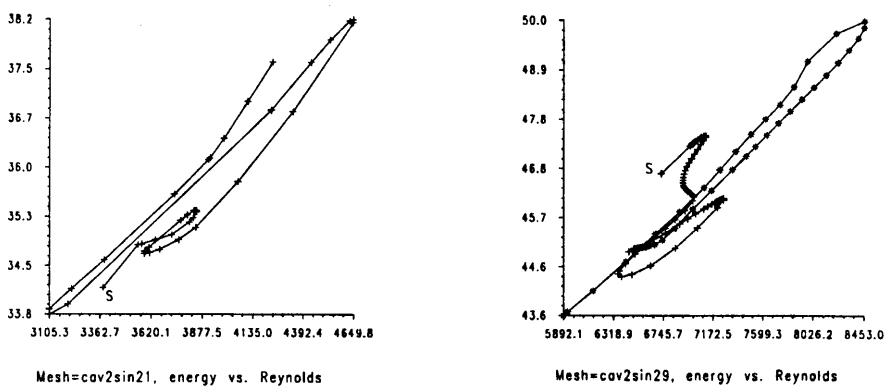

Figure 4. Bifurcation diagrams

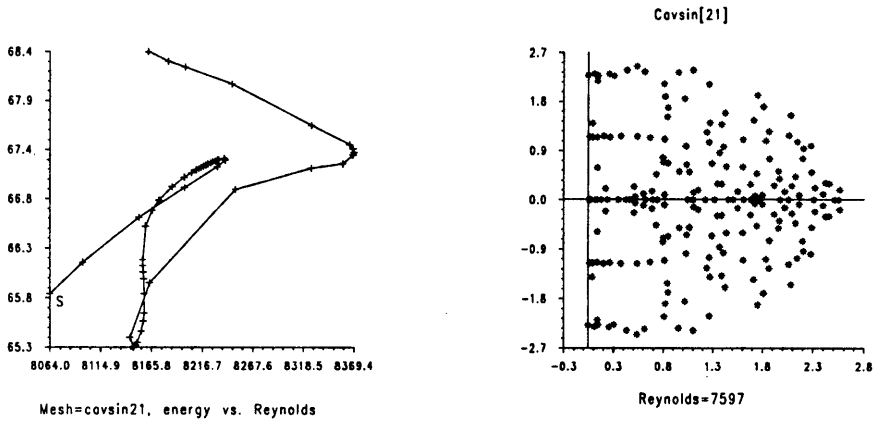

Figure 5. Bifurcation diagram (left). Spectrum for P2P1 (right)

disposed along horizontal lines at various heights ranging from zero to three for the first 250 (see Figure 7). It would be very interesting to investigate the physical meaning of this topology, but we shall not try to do that here.

For this comparison we are going to use the cavsin[21], cavsin[29] and cavsin[42] meshes and present the results obtained through monitoring of the spectrum along the curve of fundamental solutions. In contrast with the previous sections, we shall now call 'critical' the first value of $\mathscr{R}$ for which an eigenvalue crosses the imaginary axis from right to left. In all the cases to be considered, the corresponding bifurcation will be a Hopf bifurcation and the question of a correct determination of the imaginary part of the eigenvalues will be crucial. We shall begin with the P2P1 and P2P1P0 discretizations. In both cases the number of degrees of freedom (DOF) corresponding to the chosen meshes varies from 6890 to 27,890. This is basically the range for which results are given in Reference 3.

4.3.1. The P2P1 element. In Table II we present the critical values of $\mathscr{R}$ and the corresponding eigenvalues as functions of the mesh.

From Table II we remark that the limiting value of the critical Reynolds number will be in the neighbourhood of 8000 and that the limiting imaginary part of the leftmost eigenvalue tends to 2·837. Both results are in agreement with those of Reference 3. It should, however, be observed that on the cavsin[21] mesh the predicted bifurcation frequency is wrong. To get a better view of the improvement gained from mesh refinement, we represent the three corresponding spectra in Figures 5 (right) and 6.

The influence of the mesh is clear. On the coarse one the spectrum is still disorganized and the horizontal structures are not yet well defined and are wrongly situated. On the second one the structure is established and the position of the horizontal lines is correctly predicted. However, the

Table II. Critical values for P2P1

n	DOF	$\mathscr{R}_c$	σ
21	6890	7597	$0{\cdot}388 \times 10^{-3} \pm 2{\cdot}227\mathrm{i}$
29	13226	7705	$-0{\cdot}665 \times 10^{-4} \pm 2{\cdot}833\mathrm{i}$
42	27890	7960	$-0{\cdot}647 \times 10^{-3} \pm 2{\cdot}837\mathrm{i}$

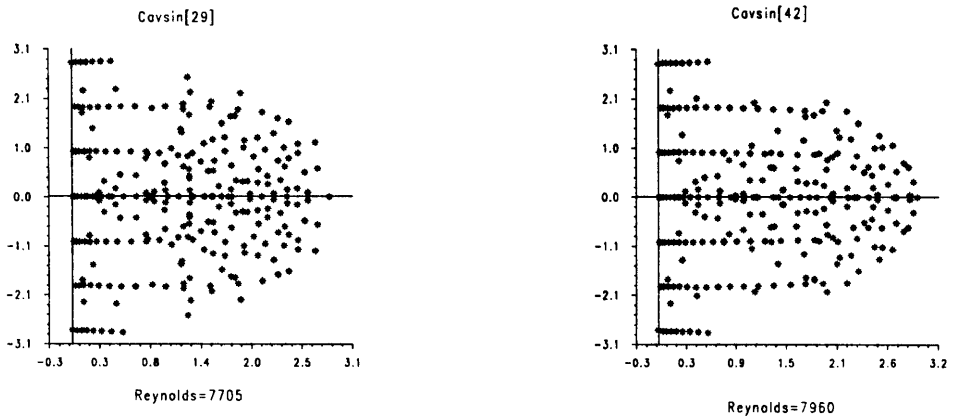

Figure 6. Spectra for P2P1

right part of the spectrum is still cloudy. One more refinement and the organization reaches that region, while the smaller structures around the real axis are stabilized. This is the structure that was obtained by Fortin *et al.*[3] and which seems to be responsible for the algorithmic difficulties that we have encountered in our eigenvalue computations. However, even if these results are satisfactory, from the finite element point of view the main difficulty is the size of the mesh required to get a good representation of the spectrum: the memory requirement is extremely high and the computational cost is enormous.

4.3.2. The P2P1P0 element. We follow the same pattern and first present a table of critical values (Table III).

Table III confirms the fact that the imaginary part of the critical eigenvalues is not very sensitive to the mesh and element parameters as long as the spectrum is properly represented. The same is not true for the critical Reynolds number, however. Indeed, with this element our limiting value goes beyond the 8000 limit suggested in Reference 3, although not by much. Memory limitation prevented us from pushing the computation further. What is this variation to be attributed to? This is not clear and we shall come back to the question a little later. The most interesting thing here is that on the coarsest mesh this discretization is able to capture the correct bifurcation. A look at the corresponding spectra, illustrated in Figure 7, confirms this.

The similarity between the spectrum generated by the P2P1P0 approximation on cavsin[21] and those given by P2P1 on cavsin[29] and cavsin[42] is striking. With half the number of degrees of freedom the first discretization is giving as good a result as the second. It is interesting to compare the numerical solutions at $\mathscr{R} = 5000$ obtained on the cavsin[21] mesh with the two discretizations. These are presented in Figure 8. Since they correctly predict the principal features of the stationary flow, they would both be considered as very acceptable, even though the P2P1P0 element does a slightly

Table III. Critical values for P2P1P0

n	DOF	$\mathscr{R}_c$	σ
21	6890	7740	$-0{\cdot}1636 \times 10^{-4} \pm 2{\cdot}876\mathrm{i}$
29	13226	7960	$-0{\cdot}1780 \times 10^{-3} \pm 2{\cdot}832\mathrm{i}$
42	27890	8040	$-0{\cdot}1620 \times 10^{-3} \pm 2{\cdot}829\mathrm{i}$

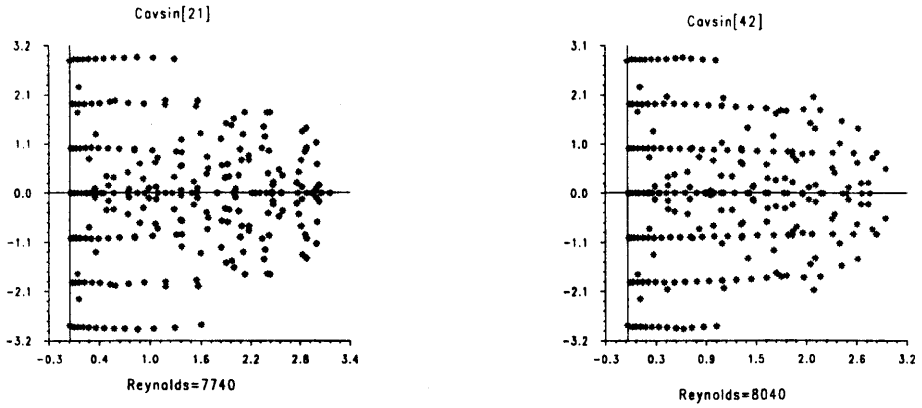

Figure 7. Spectra for P2P1P0

better job at capturing the contact zone between the main vortex and the lower right one. However, our spectral computations show that this agreement between the stationary solutions says nothing about the dynamical behaviour of the discrete systems, which, on cavsin[21], indeed behave quite differently.

In fact, a closer look at the eigenvector corresponding to the critical eigenvalue, presented in Reference 3, reveals that the main component of the perturbation responsible for the bifurcation is concentrated in the upper left corner, i.e in one of the smaller eddies, far from the main flow. Hence it appears that it is at high Reynolds number that the correct determination of the smallest structures is mandatory, and there local mass conservation is a real asset because it does not require as fine a mesh to do a good job.

4.3.3. The Mini element. We end this subsection with results obtained with the Mini element. We shall limit ourselves to the cavsin[42] mesh, for which the number of degrees of freedom (see Table I) is 21,002, which is comparable with the P2P1 case. We also recall that using Mini with one bubble function or the other is equivalent to using the SUPG scheme of Hughes and Franca;[25] thus the

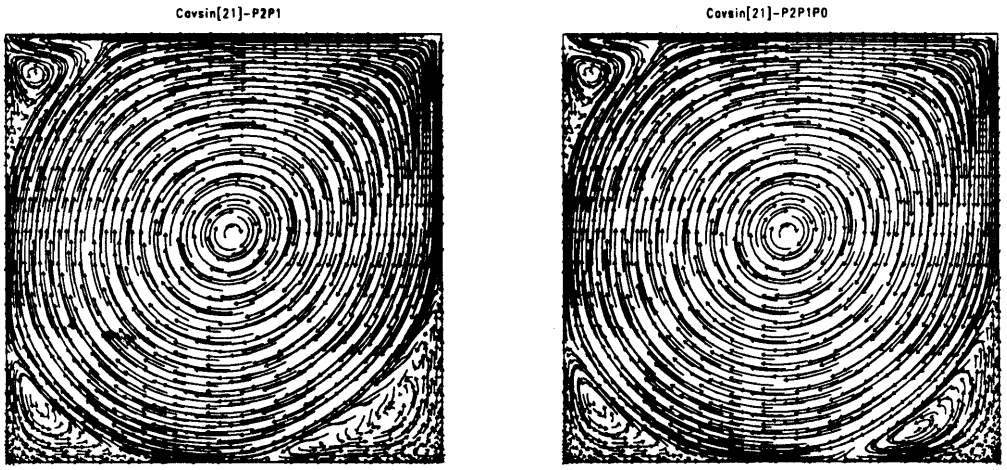

Figure 8. Solution with P2 discretizations

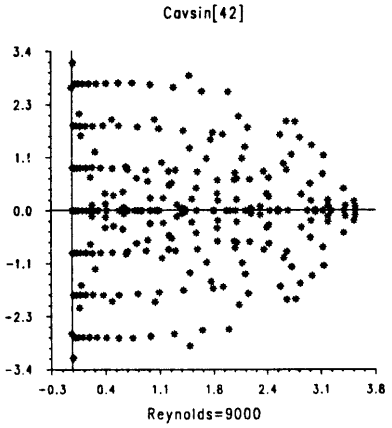

Figure 9. Spectrum for Mini

conclusion will hold also for this type of discretization. Using the cubic bubble (4) on the chosen mesh, we obtained a critical Reynolds number of about 9200, which is way beyond the range predicted by the second-order elements that we have tested. Worse, the critical eigenvalue is not correctly predicted at

$$\sigma = -0{\cdot}46 \times 10^{-3} \pm 2{\cdot}668\mathrm{i}.$$

As a matter of fact, as seen in Figure 9, the whole spectrum is affected. It has the correct structure but is somewhat shrunken in the imaginary axis direction.

We have repeated the computation with the quadratic bubble (5), which amounts to modifying the coefficients in the corresponding stabilized formulation. The results are basically the same. Hughes and Franca's work might give us a clue as to why the critical Reynolds number is so high. Indeed, since this type of discretization leads to the addition of some artificial viscosity in the streamline direction, the Reynolds number prediction is bound to be affected even though the numerical determination of the resulting perturbation might not be feasible. It is quite possible that a similar explanation holds in the P2P1 case, in that the difference between the results obtained with P2P1P0 and Q2P1 (discontinuous) used in Reference 3 might be due to numerical diffusion.

The above remarks lead us to conclude that this type of first-order spatial discretization is not appropriate for stability analysis. However, as was pointed out in Reference 7, in the Reynolds number range in which we are working, which is definitely the convection-dominated one, the stabilization parameter corresponding to either of the choices that we have made for the bubble function is not of the right order in the mesh parameter. It could be that a more drastic modification of the bubble function is called for here, as suggested in Reference 7. We have not tested this possibility, but it certainly deserves to be considered seriously in view of the interest of linear discretizations for 3D simulations.

5. CONCLUSIONS

In this paper we have studied the effect of finite element discretization characteristics on the prediction of the dynamical behaviour of the lid-driven cavity flow. Our main conclusion is twofold. First, it appears that first-order discretizations of the Mini type (or equivalently of the SUPG type) are too diffusive and that some more work is required to properly design the bubble function that should

be used at high Reynolds numbers. Second and more importantly, local mass conservation must be enforced in one way or another if one wants to obtain good results on not too overly refined meshes. In this respect, discontinuous pressure elements such as the Crouzeix–Raviart Q_2–P_1 (used in Reference 3) offer a definite advantage.

REFERENCES

1. J. W. Goodrich, K. Gustafson and K. Halasi, 'Hopf bifurcation in the driven cavity', *J. Comput. Phys.*, **90**, 219–261 (1990).
2. J. Shen, 'Hopf bifurcation of the unsteady regularized driven cavity flow', *J. Comput. Phys.*, **95**, 228–245 (1991).
3. A. Fortin, M. Jardak, J. J. Gervais and R. Pierre, 'Localization of Hopf bifurcations in fluid flow problems', *Int. j. numer. methods fluids*, in press.
4. D. N. Arnold, F. Brezzi and M. Fortin, 'A stable finite element for the Stokes equations', *Calcolo*, **21**, 337–344 (1984).
5. R. Pierre, 'Optimal selection of the bubble function in the stabilization of the P1–P1 element for the Stokes problem', *SIAM J. Numer. Anal.*, **82**, 1210–1224 (1995).
6. C. Taylor and P. Hood, 'Numerical solution of the Navier–Stokes equations using the finite element technique', *Comput. Fluids*, **1**, 1–28 (1973).
7. L. P. Franca and S. L. Frey, 'Stabilized finite element methods: II. The incompressible Navier–Stokes equations', *Comput. Methods Appl. Mech. Eng.*, **99**, 209–233 (1992).
8. P. M. Gresho, R. L. Lee, S. T. Chan and J. M. Leone, 'A new finite element for Boussinesq fluids', *Proc. Third Int. Conf. on Finite Elements in Flow Problems*, Wiley, New York, 1980, pp. 204–215.
9. D. F. Griffiths, 'The effect of pressure approximation on the finite element calculations of incompressible flows', in K. W. Morton and M. J. Baines (eds), *Numerical Methods for Fluid Dynamics*, Academic, New York, 1982, pp. 359–374.
10. R. W. Thatcher, 'Locally mass-conserving Taylor–Hood elements for two- and three-dimensional flows', *Int. j. numer. methods fluids*, **11**, 341–353 (1990).
11. R. Pierre, 'Local mass conservation and C^0-discretization of the Stokes problem', *Houston J. Math.*, **20**, 115–127 (1994).
12. A. Soulaimani, M. Fortin, Y. Ouellet, G. Dhatt and F. Bertrand, 'Simple continuous pressure elements for two- and three-dimensional incompressible flows', *Comput. Methods Appl. Mech. Engr.*, **62**, 47–69 (1987).
13. R. Schreiber and H. B. Keller, 'Driven cavity flows by efficient numerical techniques', *J. Comput. Phys.*, **49**, 310–333 (1983).
14. R. Glowinski, H. B. Keller and L. Rheinhart, 'Continuation-conjugate gradient methods for the least squares solution of nonlinear boundary value problems', *SIAM J. Sci. Stat. Comput.*, **6**, 794–832 (1985).
15. H. B. Keller, 'Numerical solution of bifurcation and nonlinear eigenvalue problems', in P. Rabinowitz (ed.), *Applications of Bifurcation Theory*, Academic, New York, 1977, pp. 359–384.
16. F. Hecht, 'Construction d'une base de fonctions $P1$ non-conformes à divergence nulle dans $\mathbb{R}^3$', RAIRO Anal. Numer., **15**, 119–150 (1981).
17. K. J. Bathe, *Finite Element Procedures in Engineering Analysis*, Prentice-Hall, Englewood Cliffs, NJ, 1982.
18. A. Fortin, M. Jardak, J. J. Gervais and R. Pierre, Old and new results on the two-dimensional Poiseuille flow, *J. Comput. Phys.*, **115**, 455–469 (1994).
19. I. S. Duff and J. A. Scott, 'Computing selected eigenvalues of sparse-unsymmetric matrices using subspace iteration', *ACM Trans. Math. Softw.*, **19**, 137–159 (1991).
20. Y. Saad, 'Chebychev acceleration techniques for solving nonsymmetric eigenvalue problems', *Math. Comput.*, **42**, 567–588 (1984).
21. D. D. Joseph, *Stability of Fluid Motions*, Vol. I, STNP Vol. 27, Springer, New York, 1976.
22. A. Georgescu, *Hydrodynamic Stability Theory*, Martinus Nijhoff, Dordrecht, 1985.
23. M. Golubitsky and D. Schaeffer, *Singularities and Groups in Bifurcation Theory*, Vol. I, Springer, New York, 1984.
24. H. K. Moffat, 'Viscous and resistive eddies near a sharp corner', *J. Fluid Mech.*, **18**, 1–18 (1964).
25. T. J. R. Hughes and L. P. Franca, 'A new finite element formulation for computational fluid dynamics: VII. The Stokes problem with various well-posed boundary conditions: symmetric formulations that converge for all velocity/pressure spaces, *Comput. Methods Appl. Mech. Eng.*, **65**, 85–96 (1987).
26. R. Schreiber and H. B. Keller, 'Spurious solutions in driven cavity calculations', *J. Comput. Phys.*, **49**, 165–172 (1983).
27. W. G. Szymczak, J. M. Solomon, A. E. Berger and J. B. Bell, 'Multiple discrete solutions of the incompressible steady-state Navier–Stokes equations', *Numer. Math.*, **53**, 31–50 (1988).
28. D. Sattinger, *Topic in Stability and Bifurcation Theory*, LNM Vol. 309, Springer, Berlin, 1973.